Pergamon

Tetrahedron 58 (2002) 787–798

TETRAHEDRON

Synthesis and conformational dynamics of *ortho*-xylyl-bridged-[4]cavitands

Christoph Naumann, Brian O. Patrick and John C. Sherman*

Department of Chemistry, University of British Columbia, 2036 Main Mall, Vancouver, BC, Canada V6T 1Z1

Dedicated to the memory of D. J. Cram

Received 13 June 2001; revised 17 September 2001; accepted 18 September 2001

Abstract—*ortho*-Xylyl-[4]cavitands **2** to **6** were synthesized from bromoresorcin[4] arenes **1**. Cavitands **2** to **6** show C_{4v} symmetry in their ^{1}H NMR spectra at higher temperatures. Dynamic ^{1}H NMR studies of **2** to **6** indicate the C_{4v} symmetry is due to fast interconversion of rectangular C_{2v} isomers. This is supported by the crystal structure of **2a**, which shows a C_{2v} rectangular structure. The activation energy barriers for **2a** and **2b** were measured by quantitative 1D NOESY (EXSY) experiments. The results were analyzed by the initial rate approximation and matrix calculations. The activation energy barrier was found to depend strongly on the size of the upper rim group (Br, H, OH, CN). In addition, replacing the phenolic proton of tetrol derivatives **4a** and **4b** with metal ions raises the energy barrier further, likely via bridging metal cations. The two tetrabromo compounds (**2a** and **2b**) reveal a sensitivity of the activation barrier to the feet of the cavitands. Cavitand **6** may act as a hub for radially expanded cavitands. The advantages of the 1D NOESY experiments over the more commonly used two-dimensional experiments are discussed.

1. Introduction

Cavitands are rigid organic host molecules that are shaped like bowls and manifest enforced cavities capable of binding to neutral guest molecules. They have been used as hosts in their own right, and as components to form carceplexes, hemicarceplexes, capsules, and related host species. Cavitands are derived from resorcinarenes, and are prepared by linking the hydroxyl groups of resorcinarenes with bridges containing 1–3 carbon units. Most common is the methylene linkage, but ethylene, propylene, and *o*-arenes have been used as well. The nature of the interbowl linker defines the volume and character of the cavity, as well as the guest(s) that will be recognized.[1] In recent years, efforts have been made to use cavitands to create larger cavities.[1] One approach is to link together several cavitands.[1,2] Another route is to extend the walls via the bridging unit.[1,3] Thus, Cram synthesized 'kites' and 'vases' using *o*-arenes as bridges. The vases and related species have been extensively elaborated by Rebek and coworkers in their studies of deep cavity cavitands (DCCs).[4,5] Gibb has used benzal bridges to create DCCs that hold promise for the creation of large container compounds.[6] Very recently, we described the expansion of cavitand chemistry using more than four resorcinol units per cavitand.[7] Here, we report an investigation of bridging resorcinarenes with *ortho*-xylyl linkers to create a new family of cavitands that are bridged with four carbon linkers and manifest novel conformational properties. Although the conformational freedom compromises the cavity to some extent, these compounds have potential as hubs for radially expanded hosts.

2. Results and discussion

2.1. Bromo-*o*-xylyl cavitands 2a and 2b

2.1.1. Synthesis and chemical shifts. Bromo-*o*-xylyl cavitands **2a** and **2b** were synthesized by standard resorcinarene bridging methods in 20–25% yield. The tetrabromo cavitand **2a** was successfully transformed into the tetranitrile and tetrahydroxy derivatives **3** (50% yield) and **4a** (25% yield) (Fig. 1) using standard methods, as were the tetrahydroxy and tetraprotio derivatives **4b**, **5a** and **5b**. ^{1}H NMR spectra of compounds **2** to **6** show C_{4v} symmetry at different (higher) temperatures. Table 1 contains a summary of the chemical shifts observed for most resonances of **2** to **6**, (see Fig. 1 for labels). In addition to the differences caused by different rim functional groups (for X, see Fig. 1), the presence of eight arenes produce a range of shielding/deshielding effects on the host protons as each host has a unique conformation. The most pronounced effects are on the *para* aromatic protons (for **2** to **6**, $H_{5,7}$, $\Delta\delta$=0.74 ppm) and the methine protons (H_{11}, $\Delta\delta$=1.34 ppm).

2.1.2. ^{1}H NMR structure of 2a. Modelling indicates a rectangular structure for **2a**, and at low temperature in CD_2Cl_2, ^{1}H NMR evidence for a C_{2v} structure was found (Fig. 2b). At −73°C at 500 MHz, the three aromatic protons

Keywords: cavitands; dynamic ^{1}H NMR; exchange; 1D NOESY (EXSY).
* Corresponding author; e-mail: sherman@chem.ubc.ca

0040–4020/02/$ - see front matter
PII: S0040-4020(01)01105-X

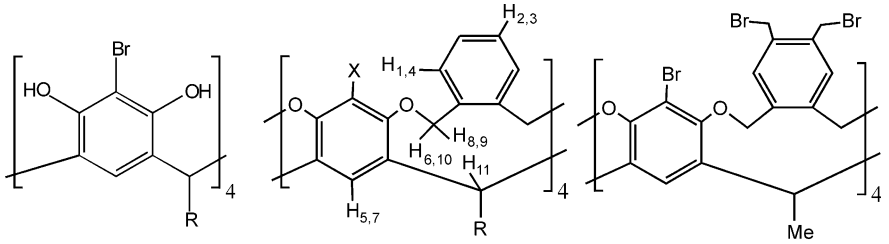

Figure 1. Schematical drawings of compounds **1**–**6**.

give rise to six different resonances (Fig. 2b, see labelling of protons in Fig. 3), which clearly indicates that the C_{4v} symmetry has been broken. The two resonances for the protons *para* to the bromines, come at 6.81 ppm (H_5) and at 5.49 ppm (H_7). The upfield shift for H_7 indicates that it points inside the cavity, as shown in Fig. 3. The other aromatic resonances correspond to 4H each as do the benzylic methylenes (H_6, H_8 to H_{10}). COSY correlations at −73°C link the aromatic xylyl protons to each other, confirming that H_1–H_4 are protons at the same aromatic unit. H_6 and H_9 are geminal protons with a coupling constant of 11 Hz, 2 Hz smaller than the one measured for H_8 and H_{10}. The methine protons (H_{11}) as well as the methyl feet protons appear as slightly broad signals. 2D NOESY NMR at the same temperature shows all correlations are negative (same phased as the diagonal). 2D ROESY NMR at −73°C shows that no exchange can be detected at that temperature; therefore all correlations at −73°C are due to NOE, not exchange. Strong NOEs are found between H_1 and H_6, and H_4 and H_{10} (see Figs. 2c and 3a).[8] There is also a medium strength NOE between the two *para* resonances H_5 and H_7. There is no NOE between H_1 and H_4, but there are strong NOEs between H_1 and H_2, H_2 and H_3, and H_3 and H_4. Weak NOEs are observed between the methine protons (H_{11}) and (H_6/H_9), and even smaller NOEs are seen between H_{11} and (H_8/H_{10}). Although both H_6/H_9 and H_8/H_{10} are predicted to point above the rim of the cavity, away from

Table 1. Chemical Shifts of key protons for C_{4v} structures of *o*-xylyl-bridged cavitands

	H_1, H_4	H_2, H_3	H_5, H_7	H_6, H_{10}	H_8, H_9	H_{11}
2a[a]	7.36		6.4 (br)	5.4 (br)	4.97	3.97
2a[b]	7.31		6.42	5.46	4.78	4.12
2b[a]	7.48		6.49	5.48	5.21	4.00
3[a]	7.49	7.45	6.99	5.57	5.25	4.42
4a[a]	7.34		6.31	5.36	4.48	4.36
4a[c]	7.36	7.32	6.34	5.37	4.71	4.33
4a[d]	7.38	7.36	6.25	5.32	4.84	4.21
4a[e]	7.45	7.33	6.96	5.63	4.86	5.08
4a[f]	7.40	7.18	6.78	5.48	4.75	5.12
4b[g]	7.42–7.36		6.71	5.39	4.73	4.67
5a[g]	7.56	7.45	6.81	5.11	4.76	5.31
5b[g]	7.58	7.48	6.89	5.14	4.78	5.27
6[h]	7.08	–	6.46	5.46	4.60	4.2

[a] CD_2Cl_2 at 27°C at 500 MHz.
[b] $CDCl_3$ at 57°C at 500 MHz.
[c] CD_2Cl_2/MeOD=1:1 at 27°C at 400 MHz.
[d] CD_2Cl_2/MeOD=1:1 at −36°C at 400 MHz.
[e] CD_2Cl_2, 1,8-diazabicyclo[5.4.0] undecene-7 (DBU) at 27°C at 500 MHz.
[f] CD_2Cl_2/MeOD, DBU at −36°C at 400 MHz.
[g] $CDCl_3$ at 27°C at 400 MHz.
[h] Toluene-d_8 at 97°C at 500 MHz.

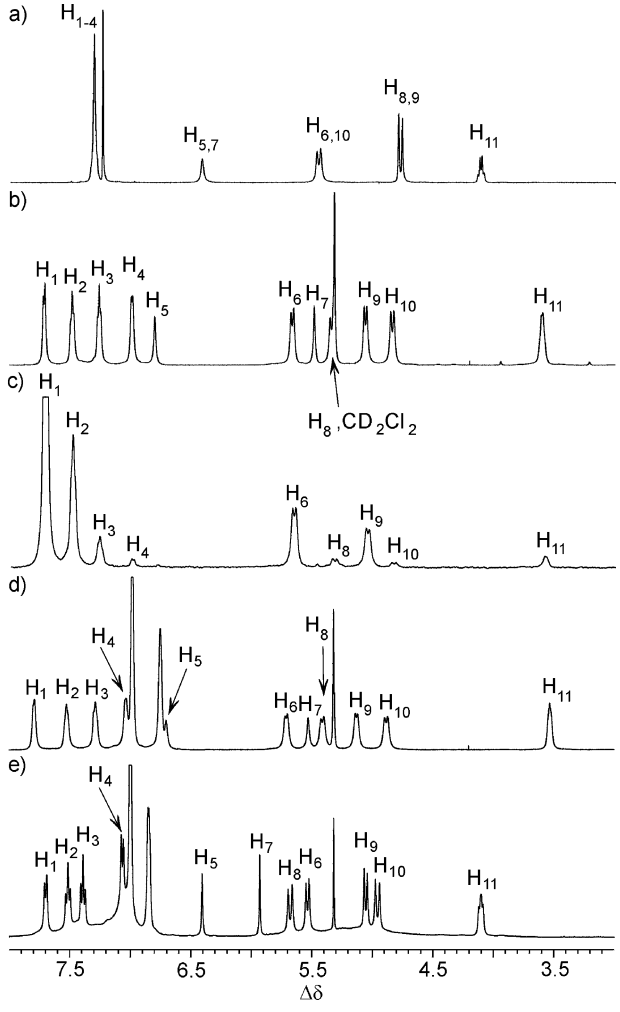

Figure 2. Parts of the ^{1}H NMR spectra of cavitands **2a** and **2b** and **4b**–CD_2Cl_2–Cs_2CO_3: (a) **2a**, in $CDCl_3$ at 57°C at 400 MHz, (b) **2a**, in CD_2Cl_2 at −73°C at 500 MHz, (c) 1D-NOESY spectra of **2a** at −83°C at 400 MHz, H_1 was irradiated, (d) **2b**, in CD_2Cl_2 at −73°C at 500 MHz, and (e) **4b**–CD_2Cl_2–Cs_2CO_3, at 28°C at 400 MHz.

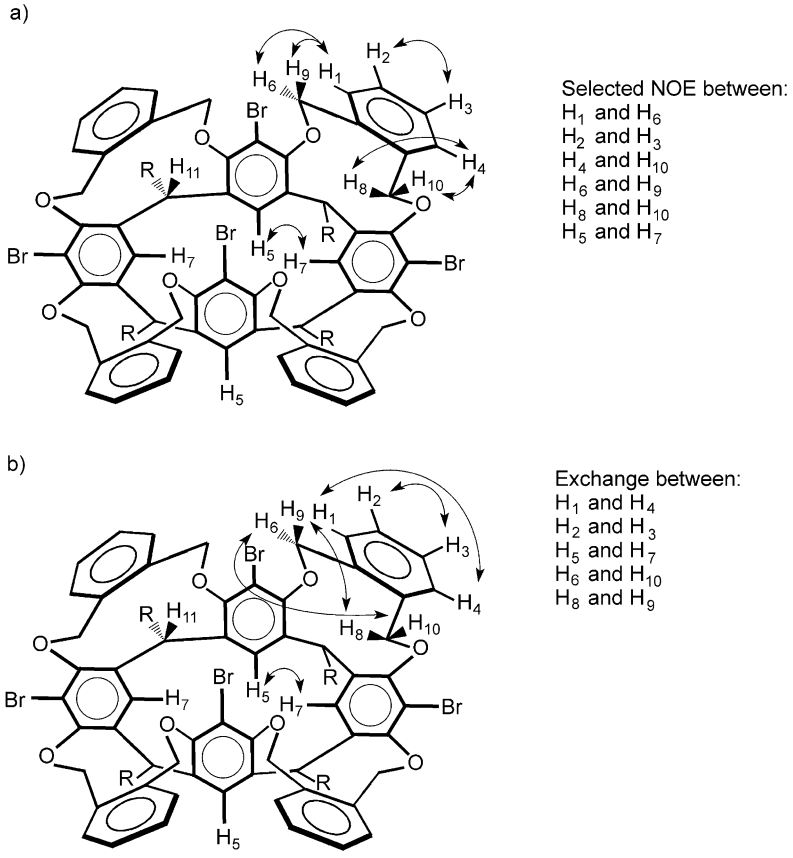

Figure 3. Summary of results of dynamic ^{1}H NMR studies on cavitands **2a** and **2b**: (a) selected NOEs, (b) Site-exchange.

the methine protons (H_{11}), CPK models indicate that H_6 and H_9 are conformationally mobile enough to spend part of their time near the methine protons. In contrast, H_8/H_{10} cannot be rotated around the neighbouring oxygen atom without great strain to the molecule, according to CPK models. There is only a very small NOE between H_6 and H_{10} and a bigger one between H_6 and H_8. Similarly, the NOE between H_8 and H_9 is bigger than the one between H_9 and H_{10}. We can conclude that of the four benzylic methylene protons, H_6 and H_{10} are farthest apart in space from each other.

2.1.3. ^{1}H NMR structure of 2b. On repeating the above experiments at the same temperature (−73°C) for tetrabromo derivative **2b**, the same C_{2v} structure is revealed. The chemical shifts for **2b** are almost identical to those for **2a** with the exception of feet related protons (Fig. 2d and Table 2).[9] COSY correlations confirm the assignments of **2a**. 2D ROESY NMR shows strong negative signals, which indicates exchange, in addition to the positive NOEs. There is exchange between H_1 and H_4, H_2 and H_3, H_5 and H_7, H_6 and H_{10}, and H_8 and H_9 (Fig. 3b, R=CH_2CH_2Ph, and Scheme 1). These exchanges confirm the assignments (for **2b** and thus by analogy for **2a**). We obtained the crystal structure of **2a** which shows a rectangular C_{2v} structure that is consistent with the NMR data and predictions from models (Fig. 4a).

2.1.4. Dynamic conformations of 2a and 2b. The fact that **2b** exchanges at a temperature where **2a** does not means that the activation energy barrier is higher for **2a** than for **2b**. 1D NOESY experiments were recorded to measure the activation barriers for both molecules.[8,10] We recently reported the use of 1D NOESY experiments to determine exchange rates.[7] Because most dynamic studies described in the literature are still based on 2D NOESY (EXSY) experiments, we provide some details in our Experimental Section on 1D NOESY experiments (both technical details and a

Table 2. Chemical shifts for C_{2v} cavitands (see Fig. 3 for labelling)

	H_1	H_2	H_3	H_4	H_5	H_6	H_7	H_8	H_9	H_{10}	H_{11}
2a[a]	7.72	7.49	7.26	6.99	6.81	5.67	5.49	5.35	5.06	4.84	3.60
2b[a]	7.79	7.53	7.29	7.03	6.70	5.71	5.53	5.41	5.13	4.88	3.53
4a[b]	7.64	7.48	7.35	7.01	6.47	5.46	5.92	5.63	4.96	4.92	4.16
4a[c]	7.68	7.42	7.27	7.19	6.29	5.72	5.40	5.52	4.85	5.00	4.05
4b[b]	7.70	7.51	7.38	7.06	6.40	5.53	5.92	5.67	5.04	4.95	4.09

[a] CD_2Cl_2 at −73°C at 500 MHz.
[b] CD_2Cl_2, Cs_2CO_3 (excess) at 27°C at 400 MHz.
[c] CD_2Cl_2/MeOD=1:1, Cs_2CO_3, −36°C at 400 MHz.

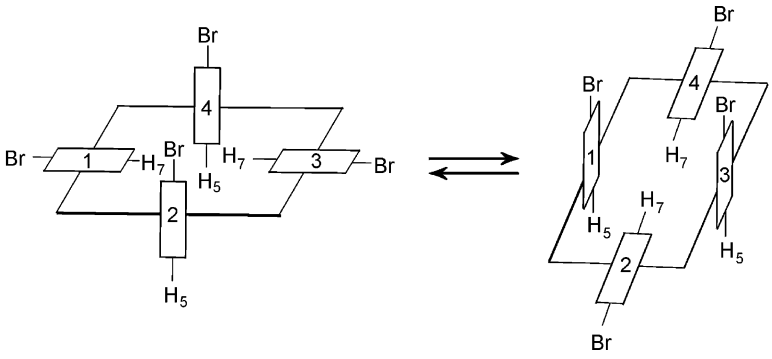

Scheme 1. Interconversion of C_{2v} conformers for **2a** and **2b**.

discussion of the advantages of 1D NOESY over 2D NOESY), as applied to the current situation, the conformational interconversion of compounds **2a** and **2b**.

At 400 MHz, the rate constants for the exchange between H_1 and H_4 and the one between H_2 and H_3 were determined for cavitand **2a** at −60°C. At that temperature, the exchange occurs sufficiently fast and the NOE build-up rates are minimized. This is especially important for exchanging protons H_2 and H_3 that can have strong NOEs to each other. For the exchange between H_1 and H_4, we also determined the rate constants at −69 and −40°C. For cavitand **2b**, we settled on −75°C as a compromise temperature: at lower temperature, the NOEs are too strong whereas at higher temperature, the exchange is too fast to measure accurately (see Experimental). The NOE contribution was stronger than for **2a** at −60°C, but the measured rate was already 10 times as fast as the one for **2a** at −60°C. Fig. 5 shows two 1D NOESY experiments for cavitand **2a**. H_1 and H_4 were irradiated at a mixing time of 0.25 s at −60°C.

To extract rate constants, the ratio between response to irradiated peak is plotted against short mixing times for the initial rate approach.[11] The slope corresponds to the rate constant. Fig. 6 shows the graphs for the two compounds **2a** and **2b** at different temperatures. For **2a** (at −69, −60, and −40°C), H_1 was irradiated, and the response occurs at H_4 (see Table 3 for a summary). For **2b** (at −75°C), H_6 was irradiated and the response occurs at H_{10}.

The free energy of activation for **2a** at −60°C was determined to be 12.2 kcal mol^{-1}, and for **2b** at −75°C

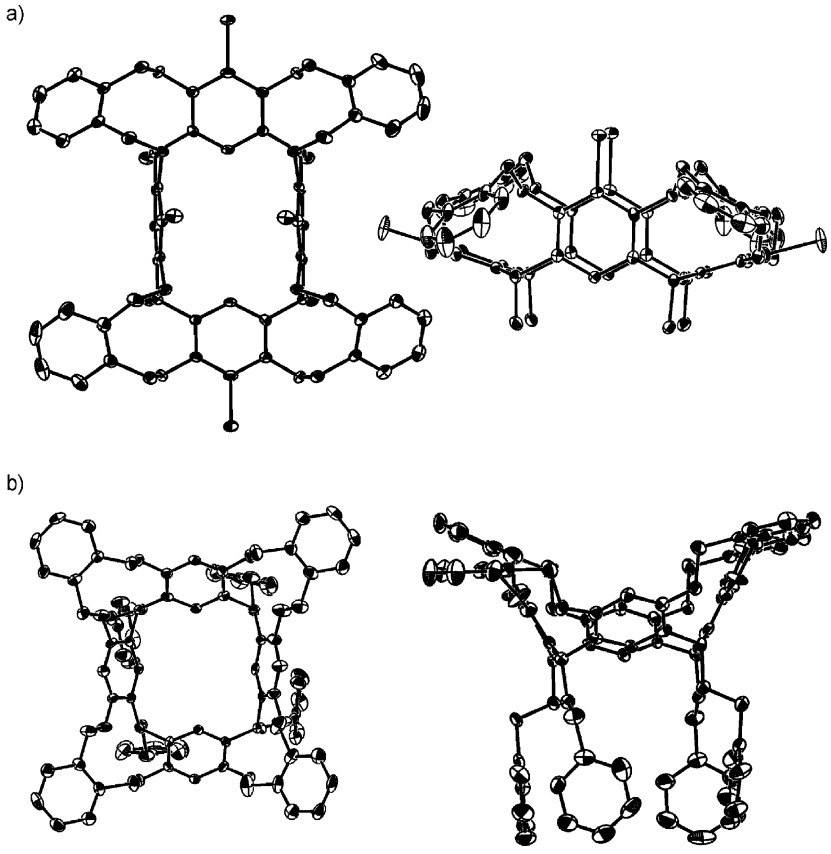

Figure 4. ORTEP plots of the X-ray crystal structures of **2a** and **5b**. Hydrogens are omitted for clarity: (a) **2a**, top and side-view, (b) **5b**, top and side-view.

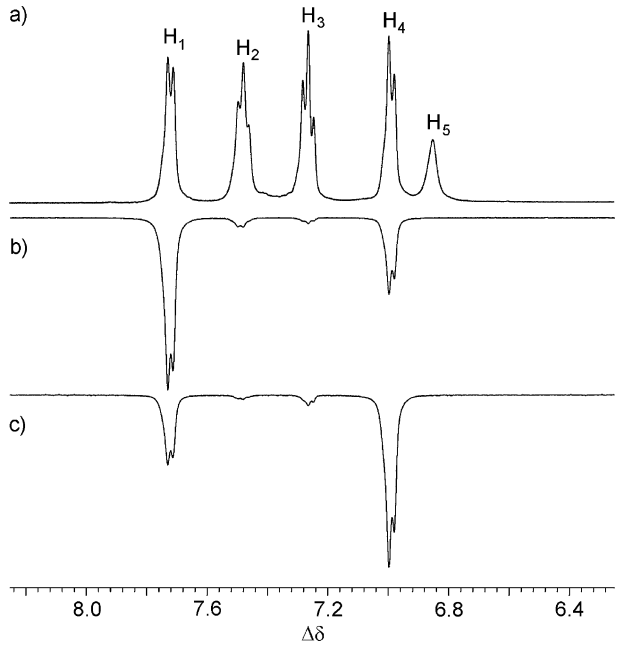

Figure 5. Parts of 1D NOESY (EXSY) spectra for cavitand **2a** at −60°C at 400 MHz: (a) no irradiation, (b) H_1 was irradiated, (c) H_4 was irradiated.

10.4 kcal mol^{-1}.[12] The difference in energy corresponds to a 60 times larger rate constant for **2b** than for **2a** at the same temperature, assuming that the activation energy barrier does not change within that small temperature change. That assumption is reasonable since intermolecular exchange often has an entropy of activation that is close to zero. Also for **2a**, data from −40 to −69°C are almost the same. Why would the phenethyl-footed cavitand have a lower activation energy? π−π interactions between the feet and the bridges may lower the transition state. More likely though, the bulky phenethyls raise the ground state toward the C_{4v} conformation of the cavitand relative to the methyl footed cavitand.

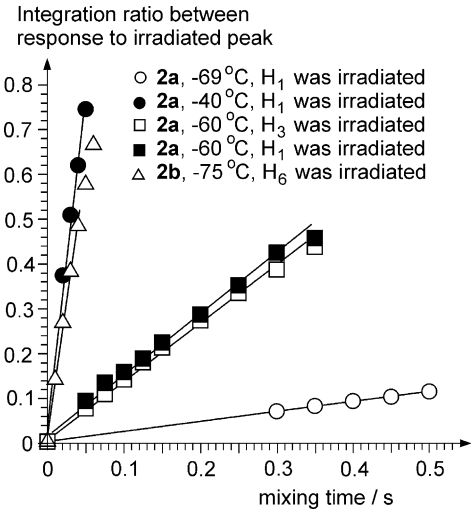

Figure 6. Graphs of the integration ratio between response to irradiated peaks of 1D NOESY spectra for cavitands **2a** and **2b** versus mixing time at different temperatures at 400 MHz. The slope for the linear initial parts corresponds to the rate constants (see Table 2 for more details).

2.2. Dynamics of cavitands with functionalized rims other than bromine

The size and character of the X group (Fig. 1) is decisive for the height of the activation barrier. Whereas the C_{4v} symmetric ^{1}H NMR spectra of **5a**,**b** (X=H), and **3** (X=CN) do not even broaden at −73°C at 500 MHz in CD_2Cl_2, the spectrum of **4a** (X=OH) is significantly broad at that temperature, comparable to **2a** (X=Br) at about −20°C. Near the freezing point of CD_2Cl_2, at −93°C at 400 MHz, the ^{1}H NMR spectrum of **4a** looks like a broad C_{2v} structure. Based on an estimated rate constant of between 50 and 100 s^{-1} at −93°C, we determined the activation barrier for **4a** to be 8.5–9.0 kcal mol^{-1}; the barrier is even lower for the other derivatives (**3**, **5a**,**b**). We obtained the crystal structure for **5b** which shows an almost C_{4v} structure (see Fig. 4b). With smaller X, the C_{4v} transition state is more easily reached, as the ground state is raised and the transition state itself may be lowered.

Addition of excess cesium carbonate to a dichloromethane solution of **4a** (or **4b**) gave a significant change in the ^{1}H NMR spectrum at room temperature: a C_{2v} structure was formed, similar to the one formed by cavitands **2a** and **2b** at low temperatures (Fig. 2d, see Table 2).[13] The same set of exchanging resonances as for **2a** and **2b** are observed (Fig. 3), although the chemical shifts for some resonances differ due to the greater degree of freedom of the benzylic protons (H_6, H_8–H_{10}) next to phenoxides in **4a** and **4b** versus bromines in **2a** and **2b**.[14]

We determined the activation barrier for interconversion (exchange of H_1 and H_4) of **4a**– and **4b**–CD_2Cl_2–Cs_2CO_3 at different temperatures (see Table 4). Addition of cesium carbonate to a CD_2Cl_2 solution of **4a** or **4b** yields $\Delta G^{\ddagger}$ of 17.6 kcal mol^{-1} at 32°C and 28°C, respectively, which represents an increase of more than 8.5 kcal mol^{-1} over **4a** or **4b** alone.

2.2.1. Solvent effects. When instead of pure CD_2Cl_2 a mixture of CD_2Cl_2:MeOD=10:1 (by volumes) was used, the activation barrier dropped significantly, to 14.2 kcal mol^{-1}. The rate constant for the exchange between H_1 and H_4 at −26°C was found to be 1.4 s^{-1}; more methanol yields lower activation barriers.[15] When potassium carbonate was used as base, similar rate constants were obtained. Other carbonate bases such as Na_2CO_3, Li_2CO_3, and $BaCO_3$ did not show any changes to the NMR spectra even in pure methanol solution when presumably some amount of base is solubilized. The activation barrier for the interconversion when pure methanol was used was found to be 11.4 kcal mol^{-1} (K_2CO_3, at −69°C) and 11.6 kcal mol^{-1} (Cs_2CO_3, −65°C), still at least 2.5 kcal mol^{-1} higher than without base. Table 4 summarizes the solvent effects on the interconversion rate constants.

2.2.2. Effects of increasing the potassium concentration in CD_2Cl_2:MeOD=1:1 solvent. We noticed that larger amounts of K_2CO_3 in CD_2Cl_2:MeOD=1:1 solvent led to somewhat higher activation barriers although we could not tell how much base was actually dissolved. We decided to use a base soluble in organic solvents. Addition of 1,8-diazabicyclo[5.4.0]undecene-7 (DBU) to a CD_2Cl_2:MeOD =1:1

Table 3. Summary of 1D NOESY experiments of compounds **2a** and **2b**

Compound	T (°C)	Irradiated proton	t_m (ms)[a]	k (s^{-1})	r	$\Delta G^{\ddagger}$ (kcal mol^{-1})
2a	−69	H_1	0–500	0.227±0.002	0.9999	12.4±0.1
2a	−60	H_1	0–150	1.41±0.02	0.9997	12.2±0.1
2a	−60	H_4	0–150	1.48±0.01	1	12.2±0.1
2a	−60	H_2	50–350	1.21±0.03	0.9983	12.2±0.1
2a	−60	H_3	50–350	1.26±0.03	0.9981	12.2±0.1
2a	−40	H_1	20–50	12.4±0.3	0.9993	12.3±0.1
2b	−75	H_6	0–30	12.8±0.4	0.9991	10.4±0.1
2b	−75	H_{10}	0–30	13.0±0.5	0.9987	10.4±0.1
2b	−75	H_2	0–30	14.3±0.8	0.9968	10.4±0.1

[a] Mixing time range used for best-fit line. The error bars of the rate constants only reflect the quality of the fit, and not the ~20% error (see 1D NOESY appendix).

solution of **4a** at −36°C leads to large changes in chemical shifts in the ^{1}H NMR spectrum but the overall C_{4v} symmetry is retained (see Table 1, and Fig. 7). Upon further cooling, no C_{2v} conformations are frozen out. However, when KI is added to that solution, the C_{2v} structure appears gradually and the signals sharpen considerable as more KI is added (Fig. 7d).[16,17] The amount of KI affects the activation barrier: 6 equiv. (13.1 kcal mol^{-1}), 20 and 45 equiv. (13.6 kcal mol^{-1}), 130 and 215 equiv. (13.8 kcal mol^{-1}), (see Table 5).[18] When KI is added to a solution of **4a** containing no DBU, no change is observed. When other salts are added to a DBU containing solution of **4a** under identical conditions, there are two different outcomes. For salts such as $MgSO_4$ and Me_4NI no change is observed: the DBU structure is retained. Salts such as $ZnBr_2$, NaOAc, LiCl, and NH_4Cl yield the C_{4v} structure that is observed when no DBU is present, which indicates fast interconversion of the C_{2v} conformers. Addition of KI to the $ZnBr_2$/DBU and LiCl/DBU containing solutions of **4a** yields broad structures.

The use of KI has the same disadvantage as K_2CO_3: its effective concentration is not known. A potassium salt that is very soluble in CD_2Cl_2:MeOD=1:1 is potassium trifluoroacetate (KTFA). A DBU containing solution of **4b** in CD_2Cl_2:MeOD=1:1 was titrated with a solution of KTFA (in CD_2Cl_2:MeOD=1:1), and the interconversion rate was recorded at −74°C at 400 MHz. With increasing amount of potassium cations, the interconversion rate constant decreases (Fig. 8, and Table 5). For example, raising the amount of KTFA from 5.1 to 10.0 equiv., leads to a rate decrease from 5.5 to 2.9 s^{-1}. In addition, the ^{1}H NMR spectra sharpen considerably with increasing amount of K^+ as was seen for **4a**–**DBU**–**KI**.

2.2.3. Metal cation effect on activation barrier. The activation barrier for cavitand **4b** containing 9 equiv. of DBU is weakly influenced when identical amounts of CsTFA or KTFA are added. Table 6 summarizes the obtained results. The same results were found for cavitand **4a** containing similar amounts of K_2CO_3 or Cs_2CO_3 in MeOD. However, sodium, lithium, zinc, and other metal cations did not produce any C_{2v} structures.

2.2.4. Discussion of the dynamic effects seen for salt adducts of 4a and 4b. Why does the activation barrier increase by 8.5 kcal mol^{-1} when Cs_2CO_3 is added to CD_2Cl_2 solutions of **4a** or **4b**? Presumably O^-Cs^+ ion pairs are formed. Interconversion may be slower because the bulky cesium cation raises the transition state or stabilizes the C_{2v} ground state. More likely, one cesium cation bridges the two opposing 'vertical' phenoxides (Scheme 2), thus 'locking' the C_{2v} conformation. In both cases, the dissociation rate of cesium becomes rate determining. That rate is much slower in CD_2Cl_2 than in methanol due to the lower polarity of CD_2Cl_2. A faster dissociation of bound cesium lowers the activation energy for interconversion between identical C_{2v} isomers. Thus $\Delta G^{\ddagger}$ for CD_2Cl_2 solutions of $\mathbf{Cs^+}$**–4a** and $\mathbf{Cs^+}$**–4b** decreases >3.5 kcal mol^{-1} for **4a** and >6.5 kcal mol^{-1} for **4b**, in the presence of methanol. There is little or no difference in interconversion rates between potassium and cesium despite their different sizes. Sodium, lithium, and zinc may form ion pairs as well but the interconversion rates are not slowed down enough to be observed at −36°C, likely due to their smaller sizes, compared to Br, and their inability to effectively bridge opposing phenoxides.

The DBU structure may be an aggregate, which is broken up by $ZnBr_2$, LiCl, NaOAc, and NH_4Cl (to give non-cation-bridged structures), as well as by KI (to give a K^+-bridged structure). When a mixture of metal cations is present, potassium cations slow down the interconversion of the C_{2v} structures but find the lithium or zinc cations to bind competitively, so the overall ^{1}H NMR spectra look broad, likely due to the presence of a mixture of species interconverting on an intermediate timescale.

Table 4. Solvent effects of cesium salt adducts of cavitands **4a** and **4b**.

cmpd.	solvent	base	H_{irr}	T / °C	k / s^{-1}	$\Delta G^{\ddagger}$ / kcal mol^{-1}
4a	CD_2Cl_2	15 equiv. Cs_2CO_3	H_4	32	1.5	17.6
4b	CD_2Cl_2	12.8 equiv. Cs_2CO_3	H_1	28	1.1	17.6
4a	CD_2Cl_2: MeOD = 10: 1	> 20 equiv. Cs_2CO_3	H_4	−26	1.4	14.2
4a	MeOD	> 20 equiv. Cs_2CO_3	H_1	−65	2.6	11.6

Cs_2CO_3 was used in excess, and was not fully soluble even in methanol. The exact dissolved concentration of Cs_2CO_3 is not known.

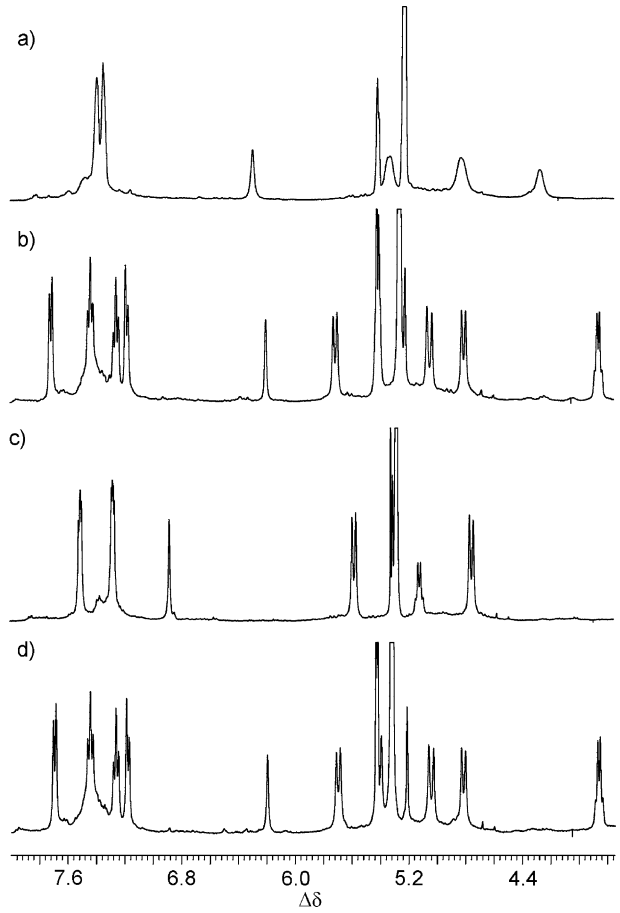

Figure 7. Parts of ^{1}H NMR spectra of **4a** in CD_2Cl_2/MeOD=1:1 at −36°C at 400 MHz: (a) **4a**, (b) **4a**+K_2CO_3 (saturated), (c) **4a**+DBU (10 equiv.), (d) addition of excess KI to (c).

Why does the interconversion rate constant of the potassium phenoxides of **4a** or **4b** decrease by increasing the amount of potassium cations, as seen for DBU/KI and DBU/KTFA? This suggests that initially several different host–guest C_{2v} complexes are formed with more or less coinciding ^{1}H NMR spectra. The observed rate constant is composed of the rate constants of the individual complexes. The addition of more potassium cations drives the equilibrium towards the complex with the highest energy barrier, thus lowering the observed rate constant and producing a more resolved ^{1}H NMR spectra.

2.3. Cavitand hub

Starting from bromoresorcin[4] arene **1a**, we also synthesized compound **6** in low yield (7%). It is interesting that a sample of **6** needs to be heated to almost 100°C in toluene-d_8 in order to interconvert the C_{2v} isomers fast enough to reach the coalesced C_{4v} structure (the spectra are too complex to perform NOESY experiments). Cavitand **6** may be coupled side-wise while the top bromines can be retained for later functionalizations. Efforts toward this aim are currently underway.

3. Conclusions and outlook

Slow interconversion on the chemical shift time-scale between identical C_{2v} isomers has been observed for tetrabromo derivatives **2a** and **2b** at low temperatures. At the same temperatures, the tetrahydroxy derivatives **4a** and **4b** show fast interconversion. Interconversion can be slowed by addition of cesium and potassium cations, which is presumably cation-bridging the C_{2v} conformers as shown in Scheme 2. We can regulate the interconversion rate of compounds **4a** and **4b** by changing the polarity of the solvent or by adjusting the concentration of potassium or cesium cations. Compound **6** may allow the expansion of cavitand chemistry sideways leading to multi-cavitand hosts or novel dendrimers. The use of 1D NOESY experiments greatly facilitates quantitative dynamic NMR studies, making them particularly accessible to supramolecular chemists.

4. Experimental

4.1. 1D NOESY Appendix

This appendix tries to summarize the strengths of 1D NOESY experiments not only for measuring rate constants but also for yielding structural information about organic molecules.[8,10]

4.1.1. Advantages of 1D NOESY (1D EXSY) over 2D NOESY (2D EXSY). 2D NOESY (EXSY)[19] experiments have one big disadvantage: they are very time-consuming.[20,21] Each quantitative experiment takes a few hours for a single mixing time. The one we determined for this work used a relaxation time of 4 s, and it took us 4 h for just

Table 5. Effects of increasing the potassium concentration in CD_2Cl_2: MeOD=1:1 solvent

cmpd.	base	H_{irr}	T / °C	k / s^{-1}	$\Delta G^{\ddagger}$ / kcal mol^{-1}
4a	35 equiv. K_2CO_3	H1	−36	3.6	13.2
4a	9 equiv. DBU, 6 equiv. KI	H_1	−36	3.8	13.1
4b	9 equiv. DBU, 45 equiv. KI	H_1	−36	1.4	13.6
4a	9 equiv. DBU, 130 equiv. KI	H_4	−36	0.91	13.8
4b	9 equiv. DBU, 4.5 equiv. KTFA	H_1	−74	5.9	10.8
4b	9 equiv. DBU, 5.1 equiv. KTFA	H_1	−74	5.5	10.8
4b	9 equiv. DBU, 6.7 equiv. KTFA	H_1	−74	4.2	10.9
4b	9 equiv. DBU, 10.0 equiv. KTFA	H_1	−74	2.9	11.1
4b	9 equiv. DBU, 20.0 equiv. KTFA	H_1	−74	1.8	11.3

KI was not fully soluble and the dissolved concentration of KI is not known. In contrast, KTFA was fully soluble.

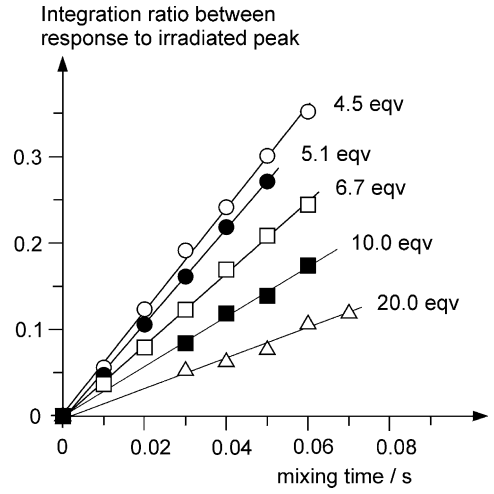

Figure 8. Graphs of the integration ratio between response to irradiated peaks of 1D NOESY spectra for cavitand **4b**–**DBU** at different concentrations of KTFA versus mixing time at −74°C (see Table 5 for details).

eight scans and 256 increments in F2. Allowing five different mixing times, 20 h of NMR time is needed. Additional time is needed in advance to decide upon the right temperature and mixing time ranges. Consider the exchange occurring in **2a** (Figs. 3 and 5, and Scheme 1). H_1 and H_4 exchange, as do H_2 and H_3. In **2a** at low temperatures, the NOEs are the same phase (negative NOEs) as the diagonal and exchange signals. If a temperature was chosen at which the exchange rate is slow, NOE build-up rates might be competing with exchange. It is essential to minimize the NOE build-up rates to obtain accurate rate constants for the interconversion. One must raise the temperature until the interconversion rates are significantly fast, and the observed NOEs are small by comparison. Exchange rates are more dependent on temperature changes than are NOE build-up rates; a change of 15°C should have a significant influence on the size of the rate constants. In addition, raising the temperature when NOEs are 'negative' (same phase as exchange and diagonal or irradiated peaks) will decrease the NOE build-up rates.[22] From our experience for different interconversions using 1D NOESY experiments, rate constants between 0.1 and 10 s^{-1} are ideal. At slower rates, NOE build-up becomes more important at the longer mixing times used. At faster rates, the mixing times become very short. Smaller rate constants (to 0.01 s^{-1}) have been obtained when there are no NOEs between the exchanging resonances.[23] 1D NOESY experiments allow the determination of approximate rate constants in a few minutes, thereby allowing one to fine tune the rate to a desired value by changing the temperature. Once a temperature has been decided upon, quantitative data can be obtained in a fraction of the time that the more commonly used 2D NOESY experiments demand. Using 1D NOESY experiments, each quantitative experiment typically takes 5–15 min for 48–128 scans at a relaxation delay (d_1) between each scan of 4 s, depending on the concentration of the sample (and on the relaxation time T_1, since $d_1=3–5\ T_1$).[24] For best results, five experiments per site are needed (five different mixing times), that is 1–2.5 h of machine time for a two-site exchange. The baseline resolution of those 1D NOESY spectra is superior to the aforementioned 2D spectrum.

4.1.2. Comparison of rate constants obtained by 1D NOESY and 2D NOESY methods. To extract rate constants from the raw data, the initial rate approximation method has been used as described in the discussion.[11] Another method to extract rate constants from exchange data is the matrix approach by Perrin et al.[20] The main reason why matrix calculations are popular is that a single mixing time can yield a rate constant (even though that is not a recommended procedure), and longer mixing times than are suitable for the initial rate approach still yield reasonable rate constants. 1D NOESY experiments save time for several different mixing times and the initial rate approximation becomes more useful.

However, matrix calculations remain useful since only they allow running a single mixing time (two 1D NOESY experiments for a two site exchange) and still be able to calculate rate constants. Applications are, for instance, measuring rate constants at a series of different temperatures, or using known exchange process as an additional control of the temperature of the probe (for an unknown exchange process).

We were also interested in comparing the results of 1D and 2D NOESY experiments. If all 1D NOESY experiments are conducted under the same conditions, and since it has been proven that 2D NOESY experiments have to be symmetric across their diagonal (even in cases of exchange between unequal populations),[25] we can reasonably treat 1D NOESY experiments as rows of 2D NOESY experiments, and use the matrix approach to extract rate constants. The two 1D NOESY spectra shown in Fig. 5 for the exchange between H_1 and H_4 of **2a** are now connected by their equal responses to the irradiation of H_1 and H_4, respectively; the irradiation of H_1 yields a response at H_4, and irradiation of H_4 under identical conditions yields a response at H_1. Both responses are normalized to one since they would be cross peaks in a two dimensional NOESY spectrum. Matrix calculation for 1D NOESY experiments on **2b** at −75°C gave a rate constant for the exchange between H_6 and H_{10} of 13.3± 0.6 s^{-1} ($\Delta G^{\ddagger}$=10.4 kcal mol^{-1}) as an average for six mixing times.[26] A single 2D NOESY experiment for **2b** at −75°C using a mixing time of 50 ms yielded a rate constant of 12.1 s^{-1} ($\Delta G^{\ddagger}$=10.4 kcal mol^{-1}). For comparison, 1D NOESY experiments at the single mixing time of 50 ms

Table 6. Metal cation effect (cesium versus potassium) in CD_2Cl_2: MeOD=1:1 solvent

cmpd.	base	H_{irr}	T / °C	k / s^{-1}	$\Delta G^{\ddagger}$ / kcal mol^{-1}
4b	12.5 equiv. Cs_2CO_3	H1	−71	5.6	11.0
4b	9 equiv. DBU, 25 equiv. CsTFA	H_1	−71	8.2	10.8
4b	9 equiv. DBU, 25 equiv. KTFA	H_1	−71	3.2	11.2

CsTFA and KTFA were both soluble, Cs_2CO_3 only partially.

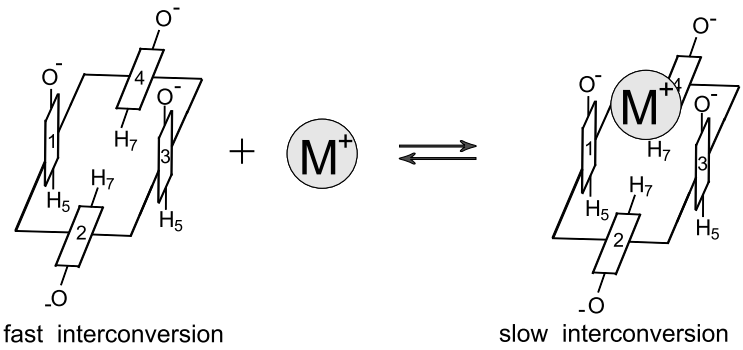

Scheme 2. Dynamic equilibrium for **4a** and **4b** in the presence of base and potassium or cesium cations.

gave a rate constant of 13.0 s^{-1} ($\Delta G^{\ddagger}$=10.4 kcal mol^{-1}). The difference is about 10%, which is within the error limits for integrating volumes in 2D NOESY spectra. Comparable values between 2D and 1D NOESY experiments were also obtained for other systems, such as [6] and [7] cavitands.[7,23]

4.1.3. Setting up 1D NOESY spectra. 1D NOESY experiments are easily set up on NMR machines that have the soft (selective) and hard (non-selective) pulses coming from the same source. If that is not the case (as on older machines), phase differences between the two sources have to be accounted for. The pulse program used is selnogp.2 (avance-version-00/02/07), a 1D NOESY experiment that uses selective refocussing with a shaped pulse.[8] Dipolar coupling may be due to NOE or chemical exchange. The widths of the selective pulses were set to 30 Hz or 0.075 ppm at 400 MHz. The 90° pulse was measured using the paropt routine. Relaxation times (T_1) were measured using the standard Bruker t1ir sequence.

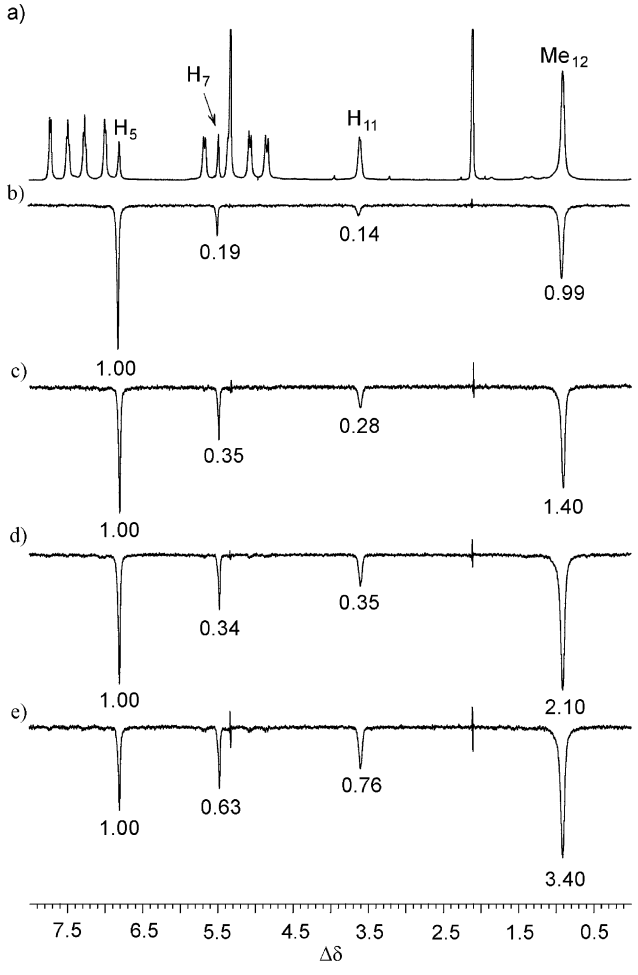

Figure 9. 1D NOESY spectra of **2a** in CD_2Cl_2 at low temperatures (b-e). H_5 was irradiated at 400 MHz. Relaxation time T_1 for H_5 is 0.9 s, and relaxation delay d_1 used between scans was 4.0 s. The numbers under the spectra (b)-(e) correspond to the integration area; (a) ^{1}H NMR spectrum at −73°C, (b) −73°C, mixing time t_m=0.4 s; (c) −73°C, t_m=0.6 s; (d) −83°C, t_m=0.4 s; (e) −83°C, t_m=0.6 s.

Samples were typically prepared in concentrations ranging from 7 to 14 mM. At a given temperature, 1D NOESY experiments were run using a few scans only and varying the mixing times to determine the range of the approximate integration ratio between irradiated peak to response. Depending on the relaxation times, each experiment takes 2 min or less. For a 1:1 exchange, the integration ratio should be 2–15. At a lower ratio, the initial rate approximation is not valid any longer; a higher ratio is too inexact to integrate. A minimum of five mixing times including the two extremes were picked. If the mixing times become long compared to the relaxation time, raising the temperature by about 10°C reduces the length of the needed range of mixing times. Similarly, lowering the temperature is recommended if the mixing times become too short. We found that using short mixing times of under 50 ms did not produce the same linearity in the obtained data as longer mixing times at a lower temperature. Adjusting the temperature may also reduce the impact of NOE build-up in case of exchanging resonances that also have NOEs to each other, here H_2 and H_3 or H_5 and H_7 (see Figs. 1 and 3 for labelling). To obtain the quantitative data, 5 min of instrument time is usually needed for each mixing time (when a relaxation delay, d_1, of 4 s is used).

4.1.4. Initial rate analysis. To obtain rate constants, the integration ratios between responding to irradiated signals is determined by integration of the processed 1D NOESY spectra. A line broadening of usually 1 Hz was imposed prior to Fourier transformation. Higher values were occasionally used for low concentration samples to obtain a better signal-to-noise ratio. A line broadening of 0.1 Hz (sometimes 0) was used for exchanging resonances that are close to each other (<0.15 ppm) to improve baseline separation for more precise integration. In general, the use of a different NMR integration program did not significantly

influence the rate constants (typically 5% variation). We recommend integrating spectra at least twice to reduce errors. We used 1D Winnmr and xwinnmr by Bruker and the two versions of MestRe-C (1.5.1, and 2.3).

The integration ratios between responding to irradiated resonances are plotted against mixing time (for instance, Figs. 6 and 8). The slope for the linear initial parts corresponds to the rate constants. We usually included zero for a mixing time zero in the calculation for the best-fit lines since no magnetization can be there at zero time. The better graphs have best-fit lines that have y-intercepts at very close to zero even without including that point into the calculations.

4.1.5. Application of 1D NOESY spectra for structural elucidation. The original purpose of selective 1D NOESY spectra has been for structural determinations of unknown compounds because small NOEs can be seen since distortions caused by difference spectra are avoided.[8] Most spatial correlations can be related by 2D NOESY spectra most of the time, except in crowded areas. For the latter cases, selective 1D NOESY spectra have a clear advantage over two-dimensional non-selective spectra since only the needed resonance can be irradiated.

The strongest NOEs can be observed under slow tumbling conditions ('negative NOEs').[27] Cavitands having molecular masses of around 1000 often show 'negative' NOEs at low temperatures and 'positive' NOEs at higher temperatures. Bigger molecules only possess 'negative' NOEs. Fig. 9 shows a series of 1D NOESY spectra obtained for **2a**. H_5 (one of the *para* aromatic protons) is irradiated at two different mixing times and temperatures. The NOEs are stronger the longer the mixing time t_m (limited by the decrease of the signal-to-noise ratio with increasing t_m), and the lower the temperature (up to the maximum 'negative' NOE of 1.0 relative to the irradiated resonance). Fig. 9 shows very strong NOEs (no exchange is seen at those temperatures).

1D NOESY spectra are clearly the better choice for quantitative measurements of NOEs (as for exchange, discussed previously).

4.1.6. Error analysis of 1D NOESY spectra. Obvious errors of 1D NOESY measurements include the errors of determining the temperature, and the integration error. We determined the temperature by measuring the chemical shift difference of standard temperature NMR samples. The temperature of the spectrometer is then determined by correlating the measured chemical shift to the true temperature using published graphs of chemical shift versus temperature for that standard sample. For low temperatures, we used a (sealed) sample of 4% methanol in methanol-d_4. The chemical shift difference between OH and CH_3 protons is measured. We determined that the error in measuring temperatures varies by no more than one degree. The integration error as judged by repeated integration of the same 1D NOESY spectrum is 10% or less.

There is an indirect way of estimating the integration error. Since the rate must be the same throughout an exchanging molecule, comparing the obtained rate constants for different exchanging resonances within the same molecule gives us a good idea of the accuracy of the 1D NOESY measurements. In the case of **2a** we are able to measure the interconversion of H_1/H_4 and H_2/H_3 resonances (Table 3). The spread of rate constants (using the initial rate analysis) ranges from 1.21 s^{-1} to 1.48 s^{-1} at −60°C. That approximate 20% range in rate constants translates into a 0.1 kcal mol^{-1} difference for $\Delta G^{\ddagger}$ (12.16–12.24 kcal mol^{-1}). Other exchanging compounds analyzed by us show the same 20% range in rate constants. However, this 20% error is quite small as compared to other dynamic NMR techniques.

4.2. Synthesis

4.2.1. Synthesis of 2a (and 2b). To a mixture of tetrabromoresorcinarene **1a** (37.0 g, 43.0 mmol) and potassium carbonate (71.7 g, 518.8 mmol) was added DMA (400 mL), and the mixture was stirred for 1 h at 60°C. α,α′-Dichloro-*o*-xylene (35.0 g, 199.9 mmol) dissolved in DMA (100 mL) was added, and the reaction was left stirring for 2 days at 60°C. After cooling to room temperature, the reaction contents were filtered through a celite plug. The filtrate was evaporated under reduced pressure. The residue was dissolved in chloroform, and subjected to column chromatography using chloroform as the eluent. Tetrabromo-*o*-xylyl-[4] cavitand **2a** was obtained as the first major product (after elution of the remaining α,α′-dichloro-*o*-xylene). It was precipitated from concentrated chloroform solutions with acetone to yield 12.2 g (9.6 mmol, 22.4%) of white powder. Cavitand **2b** was obtained by the same procedure in 25% yield.

Tetrabromo-*o*-xylyl-bowl 2a. ^{1}H NMR (500 MHz, CD_2Cl_2, 27°C): δ=7.36 (s, 16H; ArH xylyl), 6.4 (s (vbr), 4H; ArH *para*), 5.4 (s (br), 8H; $ArCH_2O$), 4.97 (d, ^2J(H,H)=12.4 Hz, 8H; $ArCH_2O$), 3.97 (q, ^3J(H,H)=6.9 Hz, 4H; Ar*CH*(CH_3)Ar), 1.09 (d, ^3J(H,H)=6.9 Hz, 12H; CH*C*H_3). ^{1}H NMR (500 MHz, CD_2Cl_2, −73°C): δ=7.72 (d, ^3J(H,H)=6.9 Hz, 4H; ArH xylyl, H_1), 7.49 (m, 4H; ArH xylyl, H_2), 7.26 (m, 4H; ArH xylyl, H_3), 6.99 (d, ^3J(H,H)=6.2 Hz, 4H; ArH xylyl, H_4), 6.81 (s, 2H; ArH *para*, H_5), 5.67 (d, ^2J(H,H)=11.0 Hz, 4H; $ArCH_2O$, H_6), 5.49 (s, 2H; ArH *para*, H_7), 5.35 (d, 4H; $ArCH_2O$, H_8), 5.06 (d, ^2J(H,H)=11.2 Hz, 4H; $ArCH_2O$, H_9), 4.84 (d, ^2J(H,H)=13.2 Hz, 4H; $ArCH_2O$, H_{10}), 3.60 (m, 4H; Ar*CH*(CH_3)Ar, H_{11}), 0.90 (m, 12H; CH*C*H_3, H_{12}). HRMS (LSIMS, thioglycerol): 1268.03674; Dev: 0.80 ppm: 64 (^{12}C), 52 (^{1}H), 8 (^{16}O), 2 (^{79}Br), 2 (^{81}Br).

Tetrabromo-*o*-xylyl-bowl 2b. ^{1}H NMR (500 MHz, CD_2Cl_2, 27°C): δ=7.48 (m, 16H; ArH xylyl), 7.10 (m, 12H; ArH feet), 6.92 (m, 8H; ArH feet), 6.49 (s, 4H; ArH *para*), 5.48 (d, ^2J(H,H)=11.8 Hz, 8H; $ArCH_2O$), 5.21 (d, ^2J(H,H)= 12.3 Hz, 8H; $ArCH_2O$), 4.00 (t, ^3J(H,H)=7.3 Hz, 4H; *methine*), 2.17 (m, 8H; CH_2CH_2Ar), 1.82 (m, 8H; $CHCH_2CH_2$). ^{1}H NMR (500 MHz, CD_2Cl_2, −73°C): δ=7.79 (s, 4H; ArH xylyl, H_1), 7.53 (s, 4H; ArH xylyl, H_2), 7.29 (s, 4H; ArH xylyl, H_3), 7.03 (s, 4H; ArH xylyl, H_4), 6.98 (s, 12H; ArH feet), 6.75 (s, 8H; ArH feet), 6.70 (s, 2H; ArH *para*, H_5), 5.71 (d (br), ^2J(H,H)=10.1 Hz, 4H; $ArCH_2O$, H_6), 5.53 (s, 2H; ArH *para*, H_7), 5.41 (d (br), ^2J(H,H)=11.6 Hz, 4H; $ArCH_2O$, H_8), 5.13 (d (br),

^2J(H,H)=9.6 Hz, 4H; $ArCH_2O$, H_9), 4.88 (d (br), ^2J(H,H)=12.2 Hz, 4H; $ArCH_2O$, H_{10}), 3.53 (m, 4H; *methine*, H_{11}), 2.01 (s (br), 4H; CH_2CH_2Ar), 1.83 (s (br), 4H; CH_2CH_2Ar), 1.59 (s (br), 4H; $CHCH_2CH_2$), 1.44 (s (br), 4H; $CHCH_2CH_2$). HRMS (LSIMS, 3-NBA): 1628.22688; Dev: 2.05 ppm: 92 (^{12}C), 76 (^1H), 8 (^{16}O), 2 (^{79}Br), 2 (^{81}Br).

4.2.2. Synthesis of tetracyano-*o*-xylyl-[4] cavitand 3. 1.00 g (0.79 mmol) of **2a**, 0.49 g (7.0 equiv.) of CuCN and NMP (13 mL) were heated in a sand bath (sand bath temperature 260°C) with stirring for 24 h. The reaction mixture was cooled to 100°C and it was poured into 30 mL of a $FeCl_3$/HCl mixture (1.25 g $FeCl_3$, 5 mL conc. HCl, 25 mL H_2O). It was heated at 100°C for 1 h. After that time, the reaction mixture was poured into water, extracted by chloroform three times, and the combined organic phases were dried and subjected to column chromatography using chloroform as the eluent. Compound **3** was obtained as a white powder (0.42 g, 0.40 mmol) in 50.5% yield.

Tetracyano-*o*-xylyl-bowl (methyl feet) 3. ^1H NMR (500 MHz, CD_2Cl_2, 27°C): δ=7.47 (m-m, 16H; ArH xylyl), 6.99 (s, 4H; ArH *para*), 5.57 (d, ^2J(H,H)=11.5 Hz, 8H; $ArCH_2O$), 5.25 (d, ^2J(H,H)=11.6 Hz, 8H; $ArCH_2O$), 4.42 (q, ^3J(H,H)=7.5 Hz, 4H; $ArCH(CH_3)Ar$), 1.30 (d, ^3J(H,H)= 7.1 Hz, 12H; $CHCH_3$). HRMS (LSIMS, thioglycerol): 1053.38643; Dev: 0.09 ppm: 68 (^{12}C), 53 (^1H), 8 (^{16}O), 4 (^{14}N).

4.2.3. Synthesis of tetrahydroxy-*o*-xylyl-[4]cavitand 4a (and 4b). 2.00 g (1.58 mmol) of **2a** was dissolved in freshly distilled THF. After cooling to −78°C, *n*-BuLi (1.6 M in hexanes, 9.9 mL, 10 equiv.) was added. After 3 min, trimethoxyborane (2.2 mL, 12 equiv.) was added to the solution. The reaction mixture was allowed to warm to room temperature. After 2 h, 100 mL of a H_2O_2/NaOH mixture (15 mL 30% H_2O_2, 85 mL 2 M NaOH) was added at −78°C. The reaction was left stirring overnight at room temperature, before the addition of NaS_2O_5 (16 g). The THF was removed under reduced pressure, and it was extracted with chloroform three times. The combined organic phases were dried and methanol (100 mL) was added. The mixture was heated with the heatgun and filtered to remove most of the less polar by-products. The filtrate was dried, dissolved in chloroform and subjected to column chromatography using chloroform as the eluent. After the remaining apolar side products had eluted, the polarity of the eluent was raised to 1% methanol–99% chloroform, and tetrol **4a** was obtained as an off-white powder. Some of the remaining (red) colour was removed by heating with methanol, and precipitating the filtrate with hexanes to obtain 410 mg of **4a** in the methanol filtrate (0.40 mmol, 25.5%). Cavitand **4b** was obtained in similar yield following the same procedure.

Tetrahydroxy-*o*-xylyl-bowl 4a. ^1H NMR (500 MHz, CD_2Cl_2, 27°C): δ=7.34 (s, 16H; ArH xylyl), 6.3 (s, 4H; ArH *para*), 5.43 (s (br), 4H; ArOH), 5.36 (d, ^2J(H,H)=12.1 Hz, 8H; $ArCH_2O$), 4.48 (d, ^2J(H,H)= 12.2 Hz, 8H; $ArCH_2O$), 4.36 (q, ^3J(H,H)=7.1 Hz, 4H; $ArCH(CH_3)Ar$), 1.33 (d, ^3J(H,H)=6.9 Hz, 12H; $CHCH_3$). HRMS (LSIMS, 3-NBA): 1017.38492; Dev: −0.08 ppm: 64 (^{12}C), 57 (^1H), 12 (^{16}O).

Tetrahydroxy-*o*-xylyl-bowl 4b. ^1H NMR (500 MHz, CD_2Cl_2, 27°C): δ=7.48 (m, 16H; ArH xylyl), 7.10 (m, 12H; ArH feet), 6.92 (m, 8H; ArH feet), 6.49 (s, 4H; ArH *para*), 5.48 (d, ^2J(H,H)=11.8 Hz, 8H; $ArCH_2O$), 5.21 (d, ^2J(H,H)=12.3 Hz, 8H; $ArCH_2O$), 4.00 (t, ^3J(H,H)=7.3 Hz, 4H; *methine*), 2.17 (m, 8H; CH_2CH_2Ar), 1.82 (m, 8H; $CHCH_2CH_2$). MS (Maldi-TOF, 4-nitroaniline): 1415 (MK^+).

4.2.4. Synthesis of tetraprotio-*o*-xylyl-[4] cavitand 5a (and 5b). 0.19 g (0.12 mmol) of **2a** was dissolved in freshly distilled THF. After cooling to −78°C, *n*-BuLi (1.6 M in hexanes, 0.7 mL, 10 equiv.) was added. After 3 min, the reaction was quenched with water and the mixture was allowed to warm up to room temperature. The crude product was purified by column chromatography using chloroform as the eluent to yield 0.13 g of **5a** (85% yield) as a white powder. Cavitand **5b** was obtained in similar yield following the same procedure.

Tetraprotio-*o*-xylyl-bowl 5a. ^1H NMR (400 MHz, $CDCl_3$, 27°C): δ=7.66 (s, 4H; ArH X-group), 7.56 (m, 8H, ArH xylyl), 7.45 (m, 8H, ArH xylyl), 6.81 (s, 4H, ArH *para*), 5.32 (q, ^3J(H,H)=7.3 Hz, 4H; $ArCH(CH_3)Ar$), 5.11 (d, ^2J(H,H)=9.5 Hz, 8H; $ArCH_2O$), 4.76 (d, ^2J(H,H)=9.1 Hz, 8H; $ArCH_2O$), 1.64 (d, ^3J(H,H)=7.7 Hz, 12H; $CHCH_3$). HRMS (LSIMS, thioglycerol): 953.40584; Dev: 0.52 ppm: 64 (^{12}C), 57 (^1H), 8 (^{16}O).

Tetraprotio-*o*-xylyl-bowl 5b. ^1H NMR (400 MHz, $CDCl_3$, 27°C): δ=7.58 (m, 12H; ArH X-group, ArH xylyl), 7.47 (m, 8H, ArH xylyl), 7.05–6.98 (m, 20H; ArH feet), 6.89 (s, 4H; ArH *para*), 5.27 (t, ^3J(H,H)=7.8 Hz, 4H; *methine*), 5.14 (d, ^2J(H,H)=9.5 Hz, 8H; $ArCH_2O$), 4.78 (d, ^2J(H,H)=9.6 Hz, 8H; $ArCH_2O$), 2.47–2.34 (m, 16H; $CHCH_2CH_2Ar$). MS (Maldi-TOF, 4-nitroaniline): 1313 (MH^+).

4.2.5. Synthesis of tetrabromo-*o*-xylyl-octabenzyl-bromide bowl (methyl feet) 6. A mixture of **1a** (2.08 g, 2.4 mmol), potassium carbonate (2.50 g, 18.1 mmol) in freshly distilled THF (75 mL) was stirred for 1 h at ambient temperature. 1,2,4,5-Tetrakis- (bromomethyl)-benzene (5.00 g, 11.1 mmol) was added, and the mixture was left stirring at ambient temperature for 4 days. After filtering through a Celite pad, and washing with toluene, the solvent was removed under reduced pressure. The residue was taken up in toluene and purified by column chromatography using toluene as the eluent. After the unreacted linker had eluted, **6** eluted, and gave a white powder (370 mg, 7.6%).

Tetrabromo-*o*-xylyl-octabenzylbromide bowl (methyl feet) 6. ^1H NMR (500 MHz, toluene-d_8, 97°C): δ=7.08 (s, 8H; ArH xylyl), 6.46 (s, 4H; ArH *para*), 5.46 (d, ^2J(H,H)=11.3 Hz, 8H; $ArCH_2O$), 4.60 (d, ^2J(H,H)= 12.3 Hz, 8H; $ArCH_2O$), 4.23 (m, 20H; $ArCH_2Br$, $ArCH(CH_3)Ar$), 1.07 (d, ^3J(H,H)=7.2 Hz, 12H; $CHCH_3$). MS (ESI): 2035 (M+Na).

4.3. X-Ray crystallography

Crystallographic data for the structures reported in this paper have been deposited with the Cambridge Crystallographic Data Centre and allocated the deposition

numbers CCDC 164982 (for **2a**) and CCDC 164983 (for **5b**). Copies of the data can be obtained free of charge on application to The Director, CCDC, 12 Union Road, Cambridge, CB2 1EZ, UK (Fax (int.): +44-1223-336-033; e-mail: deposit@ccdc.cam.ac.uk).

Acknowledgements

The authors thank NSERC for financial support.

References

1. (a) Cram, D. J.; Cram, J. M. *Container Molecules and Their Guests*, Vol. 4; Royal Society of Chemistry: Cambridge, 1994. (b) Jasat, A.; Sherman, J. C. *Chem. Rev.* **1999**, *99*, 931. (c) Makeiff, D. A.; Sherman, J. C. In *Templated Organic Synthesis*; Diederich, F., Stang, P. J., Eds.; Wiley-VCH: Weilheim, Germany, 2000; p 105. (d) Warmuth, R. *Journal of Inclusion Phenomena and Macrocyclic Chemistry* **2000**, *37*, 1. (e) Timmerman, P.; Verboom, W.; Reinhoudt, D. N. *Tetrahedron* **1996**, *52*, 2663. (f) *Calixarenes 2001*, Asfari, Z., Böhmer, V., Harrowfield, J., Vicens, J., Eds.; Kluwer Academic: Dordrecht, 2001.
2. (a) Chopra, N.; Sherman, J. C. *Angew. Chem., Int. Ed. Engl.* **1997**, *36*, 1727. (b) Chopra, N.; Sherman, J. C. *Angew. Chem., Int. Ed. Engl.* **1999**, *38*, 1995. (c) Fochi, F.; Jacopozzi, P.; Wegelius, E.; Rissanen, K.; Cozzini, P.; Marastoni, E.; Fisicaro, E.; Manini, P.; Fokkens, R.; Dalcanale, E. *J. Am. Chem. Soc.* **2001**, *123*, 7539.
3. Helgeson, R. C.; Paek, K.; Knobler, C. B.; Maverick, E. F.; Cram, D. J. *J. Am. Chem. Soc.* **1996**, *118*, 5590.
4. Moran, J. R.; Ericson, J. L.; Dalcanale, E.; Bryant, J. A.; Knobler, C. B.; Cram, D. J. *J. Am. Chem. Soc.* **1991**, *113*, 5707.
5. (a) Conn, M. M.; Rebek, Jr., J. *Chem Rev.* **1997**, *97*, 1647. For reviews of larger cavitands see: (b) Rudkevich, D. M.; Rebek, Jr., J. *Eur. J. Org. Chem.* **1999**, 1991.
6. (a) Xi, H.; Gibb, C. L. D.; Stevens, E. D.; Gibb, B. C. *Chem. Commun.* **1998**, 1743. (b) Gibb, C. L. D.; Stevens, E. D.; Gibb, B. C. *Chem. Commun.* **2000**, 363.
7. Naumann, C.; Román, E.; Peinador, C.; Ren, T.; Patrick, B. O.; Kaifer, A. E.; Sherman, J. C. *Chem. Eur. J.* **2001**, *7*, 1637.
8. Pulse sequence used: selnogp.2 (Bruker, avance-version (00/02/07): 1D NOESY using selective excitation with a shaped pulse; dipolar coupling may be due to NOE or chemical exchange. Fig. 5 shows a typical spectrum: Stott, K.; Stonehouse, J.; Keeler, J.; Hwang, T.-L.; Shaka, A. J. *J. Am. Chem. Soc.* **1995**, *117*, 4199.
9. The phenethyl protons appear as four broad singlets of four protons each, whereas the aromatic feet protons are two singlets, and the methine protons coincide too.
10. For a paper on Xenon 1D EXSY NMR see: Brotin, T.; Devic, T.; Lesage, A.; Emsley, L.; Collet, A. *Chem. Eur. J.* **2001**, *7*, 1561.
11. Kumar, A.; Wagner, G.; Ernst, R. R.; Wüthrich, K. *J. Am. Chem. Soc.* **1981**, *103*, 3654.
12. All activation energies are ± 0.1 kcal mol^{-1}, due to the low sensitivity of the activation energy to changes in the rate constants. See Experimental.
13. The solubility of Cs_2CO_3 in CD_2Cl_2 is very limited. Most of the added Cs_2CO_3 did not dissolve, and the sample (containing **4a** or **4b** and excess Cs_2CO_3) had to be warmed for 5 min to 40°C for the C_{2v} structure to appear. The addition of potassium carbonate instead of Cs_2CO_3 did not produce the C_{2v} structure possibly because of too low a solubility in CD_2Cl_2.
14. H_6 and H_9 (smaller coupling constant) as well as H_8 and H_9 (larger coupling constant) are geminal protons. H_6 and H_{10} exchange, as do H_8 and H_9. H_1 has NOE to H_6 and H_4 to H_{10}.
15. Going up to 15 vol% of MeOD yielded a rate constant of 2.3 s^{-1} at the same temperature (14.0 kcal mol^{-1}).
16. The exact amount of dissolved KI is not known.
17. Varying the amount of MeOD introduces only insignificant changes in the chemical shifts. The same is true for using K_2CO_3 or DBU/KI or DBU/potassium trifluoroacetate (KTFA) instead of Cs_2CO_3.
18. An activation energy difference of 0.7 kcal mol^{-1} corresponds to a four-fold change in rate. See Ref. 21 for a discussion of the sensitivity of k and $\Delta G^{\ddagger}$.
19. Most people use the term 'EXSY' when referring to exchange phenomena. Since the pulse sequence is 'NOESY', we prefer that nomenclature and use it for both NOE and exchange effects.
20. (a) Perrin, C. L.; Gipe, R. K. *J. Am. Chem. Soc.* **1984**, *106*, 4036. (b) Perrin, C. L.; Dwyer, T. J. *Chem. Rev.* **1990**, *90*, 935.
21. Green, M. L. H.; Wong, L.-L. *Organometallics* **1992**, *11*, 2660.
22. With 'positive' NOEs the opposite is true for cavitands; lowering the temperature may cause the NOEs to disappear but also lowers the exchange rates even faster.
23. Naumann, C.; Sherman, J. C. Unpublished results.
24. The acquisition time for each scan can be added to d_1 to yield the total relaxation delay. Many exchanging resonances have very similar T_1 values. If that is the case, even a smaller delay d_1 (e.g., $d_1=2\ T_1$) will not affect the integration ratios between irradiated to responding resonances, and will save additional machine time.
25. Willem, R. *Prog. Nucl. Magn. Reson. Spectrosc.* **1987**, *20*, 1 and Ref. 20b.
26. For **2a**, matrix calculations yield a rate constant between H_1 and H_4 of 1.46 ± 0.04 s^{-1} ($\Delta G^{\ddagger}=12.2$ kcal mol^{-1}) for nine different mixing times at -60°C (see Table 3).
27. Ernst, R. R.; Bodenhausen, G.; Wokaun, A. *Principles of Nuclear Magnetic Resonance in One and Two Dimensions*; Oxford Science Publications: Oxford, 1987.